

On the possible environmental effect in distributing heavy elements beyond individual gaseous halos

Sean D. Johnson^{1*}, Hsiao-Wen Chen¹, and John S. Mulchaey²

¹*Department of Astronomy & Astrophysics and Kavli Institute for Cosmological Physics, The University of Chicago, Chicago, IL 60637, USA*

²*The Observatories of the Carnegie Institution for Science, 813 Santa Barbara Street, Pasadena, CA 91101, USA*

4 May 2015

ABSTRACT

We present a study of extended galaxy halo gas through HI and O VI absorption over two decades in projected distance at $z \approx 0.2$. The study is based on a sample of 95 galaxies from a highly complete ($> 80\%$) survey of faint galaxies ($L > 0.1L_*$) with archival quasar absorption spectra and 53 galaxies from the literature. A clear anti-correlation is found between HI (O VI) column density and virial radius normalized projected distance, d/R_h . Strong HI (O VI) absorption systems with column densities greater than $10^{14.0}$ ($10^{13.5}$) cm^{-2} are found for 48 of 54 (36 of 42) galaxies at $d < R_h$ indicating a mean covering fraction of $\langle \kappa_{\text{HI}} \rangle = 0.89$ ($\langle \kappa_{\text{OVI}} \rangle = 0.86$). O VI absorbers are found at $d \approx R_h$, beyond the extent observed for lower ionization species. At $d/R_h = 1 - 3$ strong HI (O VI) absorption systems are found for only 7 of 43 (5 of 34) galaxies ($\langle \kappa_{\text{HI}} \rangle = 0.16$ and $\langle \kappa_{\text{OVI}} \rangle = 0.15$). Beyond $d = 3R_h$, the HI and O VI covering fractions decrease to levels consistent with coincidental systems. The high completeness of the galaxy survey enables an investigation of environmental dependence of extended gas properties. Galaxies with nearby neighbors exhibit a modest increase in O VI covering fraction at $d > R_h$ compared to isolated galaxies ($\kappa_{\text{OVI}} \approx 0.13$ versus 0.04) but no excess HI absorption. These findings suggest that environmental effects play a role in distributing heavy elements beyond the enriched gaseous halos of individual galaxies. Finally, we find that differential HI and O VI absorption between early- and late-type galaxies continues from $d < R_h$ to $d \approx 3R_h$.

Key words: galaxies: haloes – quasars: absorption lines – galaxies: interactions

1 INTRODUCTION

Galaxies grow by a combination of gas accretion from the intergalactic medium (IGM) and mergers. After heavy element enrichment, it is expected that gas is subsequently ejected back to the IGM through starburst and AGN driven winds (e.g. Murray et al. 2011) or by stripping during galaxy interactions (e.g. Wang 1993; Gauthier 2013). The low-density gas of the circum-galactic medium (CGM) is at the nexus of these baryon cycles, and it represents a potentially significant, multiphase reservoir that can fuel star-formation on long time-scales (e.g. Maller & Bullock 2004). Moreover, the CGM constitutes a sensitive laboratory for studying the physical processes that control the inflow and outflow of baryons from galaxies and for testing sub-grid feedback recipes implemented in simulations of galaxy evolution (e.g. Hummels et al. 2013; Ford et al. 2013; Cen 2013; Shen et al. 2013; Agertz & Kravtsov 2014).

The density of the CGM is nearly always too low to be

studied in emission with existing facilities. Nevertheless, a great deal of progress has been made via UV absorption-line spectroscopy of background objects at low projected distances, d , from foreground galaxies. Observations of the HI Lyman series (e.g. Chen et al. 1998; Tripp et al. 1998; Wakker & Savage 2009; Stocke et al. 2013; Rudie et al. 2013; Tumlinson et al. 2013), the Mg II doublet (e.g. Bowen et al. 1995; Chen et al. 2010; Gauthier et al. 2010; Bordoloi et al. 2011), the C IV doublet (e.g. Chen et al. 2001; Borthakur et al. 2013; Liang & Chen 2014; Bordoloi et al. 2014), and the O VI doublet (e.g. Chen & Mulchaey 2009; Wakker & Savage 2009; Prochaska et al. 2011; Tumlinson et al. 2011; Mathes et al. 2014; Stocke et al. 2014; ?) have been particularly fruitful.

Cool, metal-enriched gas traced by Mg II, C II, Si II, Si III, and C IV absorption is observed out to impact parameters of 0.7 times the galaxy virial radius ($d \approx 0.7R_h$) around both late-type and early-type galaxies of $L \lesssim L_*$ alike¹. At larger projected distances, the incidence of these

* E-mail: seanjohnson@uchicago.edu

¹ There is evidence that C IV absorption is more extended around

Table 1. Summary of galaxy and absorber properties.

Quasar sightline	Galaxy		z_{gal}	$\log(M_*/M_\odot)_{gr}$	class ^a	envi. ^b	survey	d (kpc)	d/R_h	$\log N/\text{cm}^{-2}$	
	R.A. (J2000)	Dec. (J2000)								HI ^c	O VI ^c
J0042-1037	00:42:22.27	-10:37:35.2	0.0950	9.5	Late	I	COS-Halos	15	0.1	14.80 - 18.50	14.70 ± 0.22
J0226+0015	02:26:12.98	+00:15:29.1	0.2274	10.4	Early	I	COS-Halos	81	0.4	14.36 ± 0.06	< 13.12
HE0226-4110	02:27:46.27	-40:53:15.1	0.1120	10.4	Early	I	IMACS	826	4.1	< 12.88	< 12.90
HE0226-4110	02:27:57.47	-40:57:25.7	0.2952	8.6	Late	I	IMACS	884	9.8	13.36 ± 0.05	< 12.75
HE0226-4110	02:28:01.44	-40:57:55.7	0.3863	9.8	Late	I	IMACS	846	6.5	13.39 ± 0.04	< 12.66
HE0226-4110	02:28:04.31	-40:55:57.4	0.1772	10.5	Early	NI	IMACS	435	2.1	< 12.23	< 13.07
HE0226-4110	02:28:04.52	-40:57:02.3	0.3971	11.1	Late	NI	IMACS	648	1.8	13.99 ± 0.02	13.57 ± 0.09
HE0226-4110	02:28:09.37	-40:57:44.5	0.3341	9.7	Late	NI	IMACS	346	2.6	< 12.36	< 12.75
HE0226-4110	02:28:10.23	-40:55:48.1	0.1248	8.5	Late	I	IMACS	230	2.3	12.88 ± 0.05	< 12.84
HE0226-4110	02:28:10.50	-40:58:57.3	0.3268	9.4	Early	I	IMACS	547	4.7	< 12.35	< 13.05
HE0226-4110	02:28:11.32	-40:56:36.7	0.2804	8.4	Late	I	IMACS	244	2.8	13.73 ± 0.01	-1
HE0226-4110	02:28:11.59	-40:58:53.8	0.2492	8.6	Late	I	IMACS	419	4.5	13.38 ± 0.03	< 13.16
HE0226-4110	02:28:13.89	-40:59:46.2	0.3939	10.2	Late	I	IMACS	812	5.2	< 12.36	< 12.62
HE0226-4110	02:28:14.56	-40:57:22.7	0.2065	8.9	Late	NI	IMACS	37	0.4	15.27 ± 0.06	14.37 ± 0.01
HE0226-4110	02:28:16.29	-40:57:27.2	0.2678	10.3	Early	I	IMACS	75	0.4	< 12.97	< 12.87

Notes

The full table is available in the online version of the paper.

^a Galaxy classification with “Early” for early-type, absorption-line dominated galaxies and “Late” for late-type, emission-line dominated galaxies

^b Galaxy environment class as defined in the text with “I” for isolated, “NI” for non-isolated, and “A” for ambiguous cases.

^c Total column density measured in the COS sightline within $\Delta v = \pm 300 \text{ km s}^{-1}$ of the galaxy systemic redshift. In cases where O VI or HI column densities cannot be measured due to contamination, the value is set to -1.

absorption species decreases sharply to near zero. Liang & Chen (2014) present two possible explanations for this “metal-boundary”: (1) an inability of galactic outflows and satellite accretion to efficiently deposit heavy element enriched gas at distances greater than $0.7 R_h$ or (2) an inability of cool-warm gas clouds to form and survive at larger distances.

In contrast, highly-ionized and enriched gas traced by the O VI doublet is found to reflect the bimodal distribution of galaxies in color-magnitude diagrams. In particular, strong O VI systems are found at high incidence out to $d = 150 \text{ kpc}$ around star-forming galaxies but at lower incidence around more quiescent ones (Chen & Mulchaey 2009; Tumlinson et al. 2011). Moreover, O VI detections have been reported around sub- L_* galaxies out to $d = 300 \text{ kpc}$ which corresponds to $1 - 3 R_h$ (Prochaska et al. 2011). However, the sample of galaxies probed at such large distances by absorption spectroscopy is small and the spatial extent of O VI bearing gas around galaxies remains an open question.

To examine the spatial dependence of O VI absorption around galaxies, we have assembled a sample of 95 galaxies that are probed in absorption by quasar sightlines with UV spectra from the Cosmic Origins Spectrograph (COS; Green et al. 2012) on the *Hubble Space Telescope* (HST). These galaxies are drawn from a highly complete ($\gtrsim 80\%$ complete for galaxies of $L > 0.1 L_*$ at $z < 0.4$ and $d < 500 \text{ kpc}$) survey of faint galaxies in the fields of four high signal-to-noise COS quasar sightlines. The high completeness of the galaxy survey enables a detailed investigation of possible environmental dependence of extended gas around galaxies. To increase the number of massive galaxies in the study, we include eleven galaxies with stellar masses of $\log M_*/M_\odot > 11$ from the Sloan Digital Sky Survey (SDSS; York et al. 2000) probed in absorption with archival COS quasar spectra. We

refer to these galaxy samples collectively as the extended-CGM (eCGM) survey and combine it with 42 galaxies from the COS-Halos program (Werk et al. 2012; Tumlinson et al. 2013) which are primarily at $d < 150 \text{ kpc}$. Together, the two samples contain 148 galaxies and enable an investigation of the absorption properties of galaxy halos over two decades in projected distance.

The paper proceeds as follows: In Section 2 we describe the galaxy sample. In Section 3 we describe the corresponding absorption-line measurements. In Section 4 we characterize the observed HI and O VI absorption as a function of projected distance. In Section 5 we discuss the implications of our survey results. Throughout the paper, we adopt a Λ cosmology with $\Omega_m = 0.3$, $\Omega_\Lambda = 0.7$, and $H_0 = 70 \text{ km s}^{-1} \text{ Mpc}^{-1}$.

2 THE EXTENDED-CGM GALAXY SAMPLE

To assemble the eCGM galaxy sample, we combined our own absorption-blind survey data targeting galaxies of $r_{\text{AB}} < 23 \text{ mag}$ in the fields of HE 0226-4110, PKS 0405-123, LBQS 1435-0134, and PG 1522+101 with spectroscopic galaxies in the Sloan Digital Sky Survey Data Release 10 (SDSS; York et al. 2000; Ahn et al. 2014). The HE 0226-4110, PKS 0405-123, LBQS 1435-0134, and PG 1522+101 fields were selected because of the high completeness levels ($\gtrsim 80\%$) achieved by our surveys for galaxies as faint as $L = 0.1 L_*$ at $z < 0.4$ and $d < 500 \text{ kpc}$. At smaller projected distances of $d = 100$ and 200 kpc , the survey completeness increases to 100% and 90% respectively (see Figure 2 of Johnson et al. 2013)². We included SDSS galaxies to increase the number of eCGM sample members of $\log M_*/M_\odot > 11$. The resulting galaxy sample is summarized in Table 1, and its construction is described in this section.

starburst galaxies (Borthakur et al. 2013), and more massive luminous red galaxies exhibit reduced Mg II absorption (Gauthier et al. 2010).

² Here, we adopt a characteristic luminosity of L_* galaxies of $M_r = -21.5$ based on the luminosity function measurements from Montero-Dorta & Prada (2009) and Loveday et al. (2012).

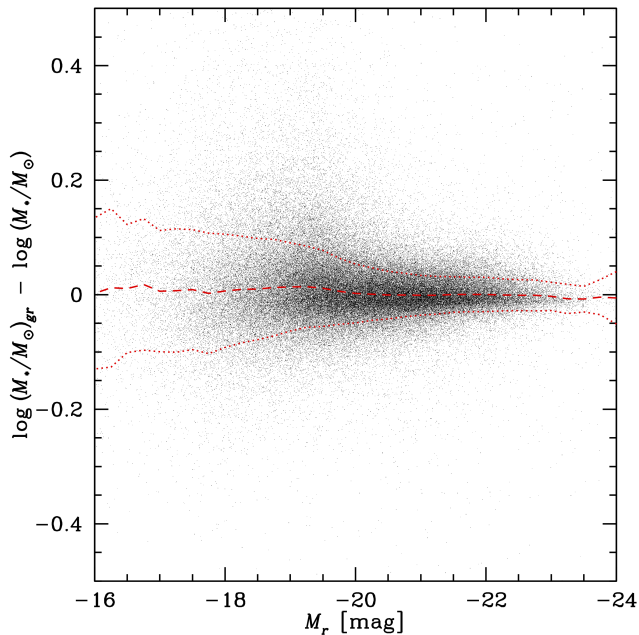


Figure 1. Residuals between rest-frame g - and r -band based stellar masses estimated using Equations 1 and 2 and those from the NASA-Sloan atlas versus absolute r -band magnitude, M_r . Each point represents a NASA-Sloan galaxy. The dashed red line shows the median residuals in M_r bins with widths of 0.25 mags. The dotted red lines mark $\pm 1\sigma$ from the median in each bin. Within the NASA-Sloan atlas, the systematic error is less than 0.02 dex with 1σ scatter of less than 0.15 dex.

Our galaxy surveys in the HE 0226-4110, PKS 0405-123, LBQS 1435-0134, and PG 1522+101 fields were carried out with the IMACS (Dressler et al. 2011) and LDSS3 spectrographs on the Magellan Telescopes (Shectman & Johns 2003) targeting galaxies as far as $\Delta\theta = 10'$ from the quasar sightline (corresponding to $d = 1.1$ Mpc at $z = 0.1$). The resulting redshift catalogs and corresponding absorption-line measurements for the HE 0226-4110, PKS 0405-123 fields were published in Chen & Mulchaey (2009) and Johnson et al. (2013). The published survey data include deep B -, V -, and R -band photometry in the HE 0226-4110 field. The LBQS 1435-0134, and PG 1522+101 galaxy redshift catalogs and corresponding IMACS g -, r -, and i -band photometry will be published in Johnson et al. in prep. For the PKS 0405-123 field, we retrieved g -, r -, and i -band images from the Mosaic II CCD Imager on the Blanco 4-m telescope from the NOAO archive (PI: Brian Keeney; PID=2008B-0194). The Mosaic II images consist of 7×75 second exposures in each bandpass. We measured the galaxy photometry using Source Extractor (Bertin & Arnouts 1996) with settings described in Johnson et al. (2014).

To increase the number of massive galaxies in the eCGM sample, we cross-matched galaxies of $\log M_*/M_\odot > 11$ in the SDSS DR10 spectroscopic survey with quasar sightlines that have public, high signal-to-noise COS spectra published in Danforth et al. (2014). For the SDSS galaxies, we adopted u -, g -, r -, i -, and z -band cmodel magnitudes³.

³ The results presented in this paper do not change if model rather than cmodel magnitudes are adopted for SDSS galaxies.

From this parent sample of galaxies, we selected those with projected distances from the quasar sightline $d < 1$ Mpc, within the redshift range $z \approx 0.1 - 0.4$, and with redshift at least $10,000 \text{ km s}^{-1}$ below the quasar redshift. O VI detections have been reported at projected distances of up to 300 kpc from sub- L_* galaxies (Prochaska et al. 2011) which corresponds to 2 – 3 times the galaxy halo virial radius. The $d = 1$ Mpc cut was chosen to be sufficiently large to search for absorption at $d/R_h = 2 - 3$ around more massive galaxies that have virial radii of $R_h \approx 300$ kpc. The redshift lower limit was chosen so that the O VI doublet falls within the COS wavelength range. We note that the redshift range for which the O VI doublet is observable with COS depends on the settings used for the observations. The redshift lower limit therefore varied slightly from sightline to sightline. The redshift upper limit was motivated by the depth of our IMACS redshift surveys which are sensitive to galaxies of $L > 0.1 L_*$ at $z \lesssim 0.4$. The requirement that the galaxy redshift be at least $10,000 \text{ km s}^{-1}$ below the quasar redshift was imposed to avoid confusion with gas outflowing from the quasar (e.g. Wild et al. 2008). In total, 106 galaxies met these criteria with eleven galaxies from the SDSS and 95 from our survey data.

For each galaxy, we measured the rest-frame, g - and r -band absolute magnitudes using the multi-band optical photometry⁴ described above and the kcorrect tool (Blanton & Roweis 2007). We then estimated mass-to-light ratios using the relation shown in Equation 1 which is a fit of the stellar mass to r -band light ratio (in solar units) for low redshift galaxies in the NASA-Sloan atlas (e.g. Maller et al. 2009). For galaxies redder than $M_g - M_r = 0.15$ in the rest-frame, the fit is a quadratic in $M_g - M_r$. For galaxies bluer than $M_g - M_r = 0.15$, we set the mass-to-light ratio to $\log(M_*/L_r) = -0.6$ which corresponds to an imposed minimum age of ≈ 0.3 Gyr for a simple stellar population with solar metallicity.

$$\log(M_*/L_r) = \begin{cases} -0.6 & M_g - M_r < 0.15 \\ -1.01 + 2.95(M_g - M_r) \dots & M_g - M_r \geq 0.15 \\ -1.67(M_g - M_r)^2 & \end{cases} \quad (1)$$

We then estimated the stellar mass of the eCGM galaxies using Equation 2 and the mass-to-light ratios from Equation 1.

$$\log(M_*/M_\odot)_{gr} = 1.872 - 0.4M_r + \log(M_*/L_r) \quad (2)$$

The rest-frame g - and r -band stellar mass estimates from Equations 1 and 2 reproduce the NASA-Sloan stellar masses which are calculated with kcorrect, a Chabrier (2003) initial mass function and GALEX $FUV + NUV$ and SDSS $ugriz$ photometry with a systematic error of less than 0.02 dex and 1σ scatter of less than 0.15 dex for galaxies of $M_r = -16$ to -24 as shown in Figure 1. The NASA-Sloan atlas contains low-redshift galaxies of $z < 0.055$ so the use of a mass-to-light ratio relation based on these galaxies for the $z = 0.1 - 0.4$ eCGM sample may result in systematic errors due to galaxy evolution over cosmic time. To estimate the magnitude of this systematic error, we compared stellar masses calculated using Equations 1 and 2 to those

⁴ Corrected for Milky Way extinction from Schlegel et al. (1998).

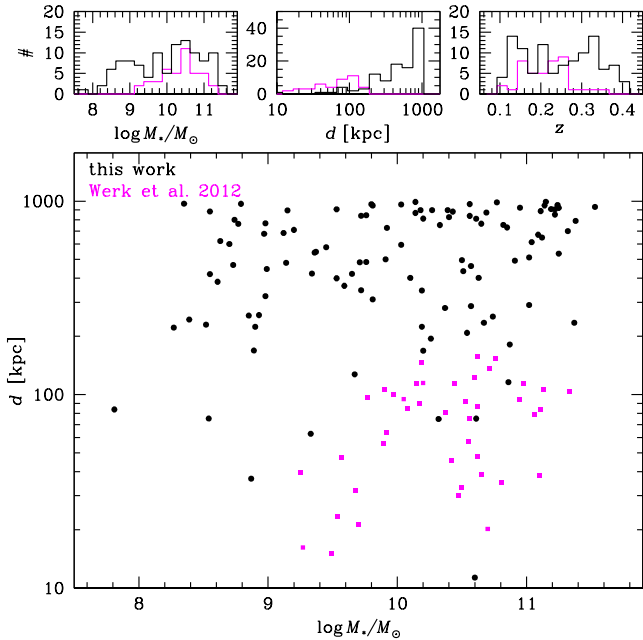


Figure 2. Distribution of projected distance, d , between each galaxy and the nearby COS quasar sightline versus stellar mass for the eCGM galaxy sample (black circles) and the COS-Halos survey (magenta squares). The *top* three panels show the stellar mass, projected distance, and redshift distributions of the eCGM and COS-Halos galaxy samples.

based on precise *ugriz* photometry for $z = 0.1 - 0.4$ galaxies from the PRIMUS galaxy survey (Coil et al. 2011). The systematic error introduced by using a $z < 0.055$ relation for $z = 0.1 - 0.4$ galaxies is less than 0.1 dex over the luminosity range spanned by the eCGM sample.

The eCGM galaxy sample spans a stellar mass range of $\log M_*/M_\odot = 8.4 - 11.5$ with a median of $\log M_*/M_\odot = 10.3$ as shown in Figure 2.

In order to compare absorption properties of galaxies across a range of stellar mass, we measured projected distance in units of the galaxy dark matter halo virial radius defined by Bryan & Norman (1998) using the stellar-to-halo mass relation from Kravtsov et al. (2014). To ensure consistency across the sample, we re-measured the virial radii of the COS-Halos galaxies using the same methods. We note that our virial radius estimates are as much as 50% smaller than those of Tumlinson et al. (2013) because of the use of a different stellar-to-halo mass relation. The differences between the stellar-to-halo mass relations from Kravtsov et al. (2014) and previous work such as Moster et al. (2010) and Behroozi et al. (2013) are driven by systematic errors in the galaxy photometry in the catalogs used by Moster et al. (2010) and Behroozi et al. (2013) (see Bernardi et al. 2013). The stellar-to-halo mass relation from Kravtsov et al. (2014) is in good agreement with independent constraints from weak lensing (e.g. Reyes et al. 2012).

To search for correlations between CGM properties and the presence of star-formation, we spectroscopically classified galaxies as late-type (emission-line dominated) and early-type (absorption-line dominated) based on a PCA fitting technique described in Chen & Mulchaey (2009). Unlike some previous surveys, we did not restrict the

eCGM galaxy sample to isolated galaxies only. Instead, we classified galaxies as “non-isolated” or “isolated” based on the presence or absence of nearby neighbors. In the HE 0226-4110, PKS 0405-123, LBQS 1435-0134, and PG 1522+101 fields, where our galaxy survey data are highly complete, we classified galaxies as “non-isolated” if they have a spectroscopic neighbor within a projected distance of less than 500 kpc, a radial velocity difference of $|\Delta v| < 300 \text{ km s}^{-1}$, and with stellar mass of at least one-third of that of the eCGM or COS-Halos survey member. Otherwise, we classified galaxies without such nearby neighbors as “isolated”.

Among non-isolated galaxies, the relevant projected distance between the quasar sightline and the galaxy is not clear a priori, and care must be taken in defining the distance to a non-isolated galaxy to prevent a bias when comparing with isolated ones. For example, a mass or light-weighted projected distance could be large even though the gas detected in absorption may be more closely associated with a less massive “group” member close to the quasar sightline. To avoid a bias that could make the gas around non-isolated galaxies appear artificially extended, we define the distance to non-isolated galaxies as the minimum value of d/R_h among “group” members. This distance definition is a self-consistent choice for comparing the spatial extent of absorbing gas around isolated and non-isolated galaxies.

The available galaxy survey data in the COS-Halos and SDSS fields are not sufficiently complete to confidently classify galaxies by environment based on spectroscopy alone. To classify these galaxies, we performed a literature search to identify members of previously known galaxy groups (e.g. McConnachie et al. 2009) and clusters (e.g. Koester et al. 2007). In addition, we visually inspected the SDSS images in the vicinity of each galaxy to search for likely neighbors based on galaxy brightness, size, color, and SDSS photometric redshift. We classified galaxies with such neighbors as non-isolated and those without as isolated.

3 ABSORPTION DATA

For each galaxy in the eCGM sample, we searched for HI and O VI absorption in the COS quasar spectra within a radial velocity interval of $\Delta v = \pm 300 \text{ km s}^{-1}$ of the galaxy systemic redshift. Tumlinson et al. (2011) found that the radial velocity distribution of O VI absorption-components around galaxies at $d < 150 \text{ kpc}$ is characterized by a standard deviation of $\sigma \approx 100 \text{ km s}^{-1}$. The $\Delta v = \pm 300 \text{ km s}^{-1}$ search window was chosen to include the vast majority of absorption associated with the eCGM and COS-Halos galaxies⁵. If HI or O VI absorption was detected, we adopted available Voigt profile fitting results from Johnson et al. (2013), Tumlinson et al. (2013), Werk et al. (2013), and Savage et al. (2014). When these measurements are not available, we performed our own Voigt profile fitting using the VPFIT package (Carswell et al. 1987) as described in Johnson et al. (2013). If HI or O VI absorption was not detected, we placed 2σ upper limits on the equivalent width, integrating over a velocity interval of 75 km s^{-1} for HI and 90

⁵ The results presented in this paper do not change if the velocity window is increased to $\Delta v = \pm 600 \text{ km s}^{-1}$.

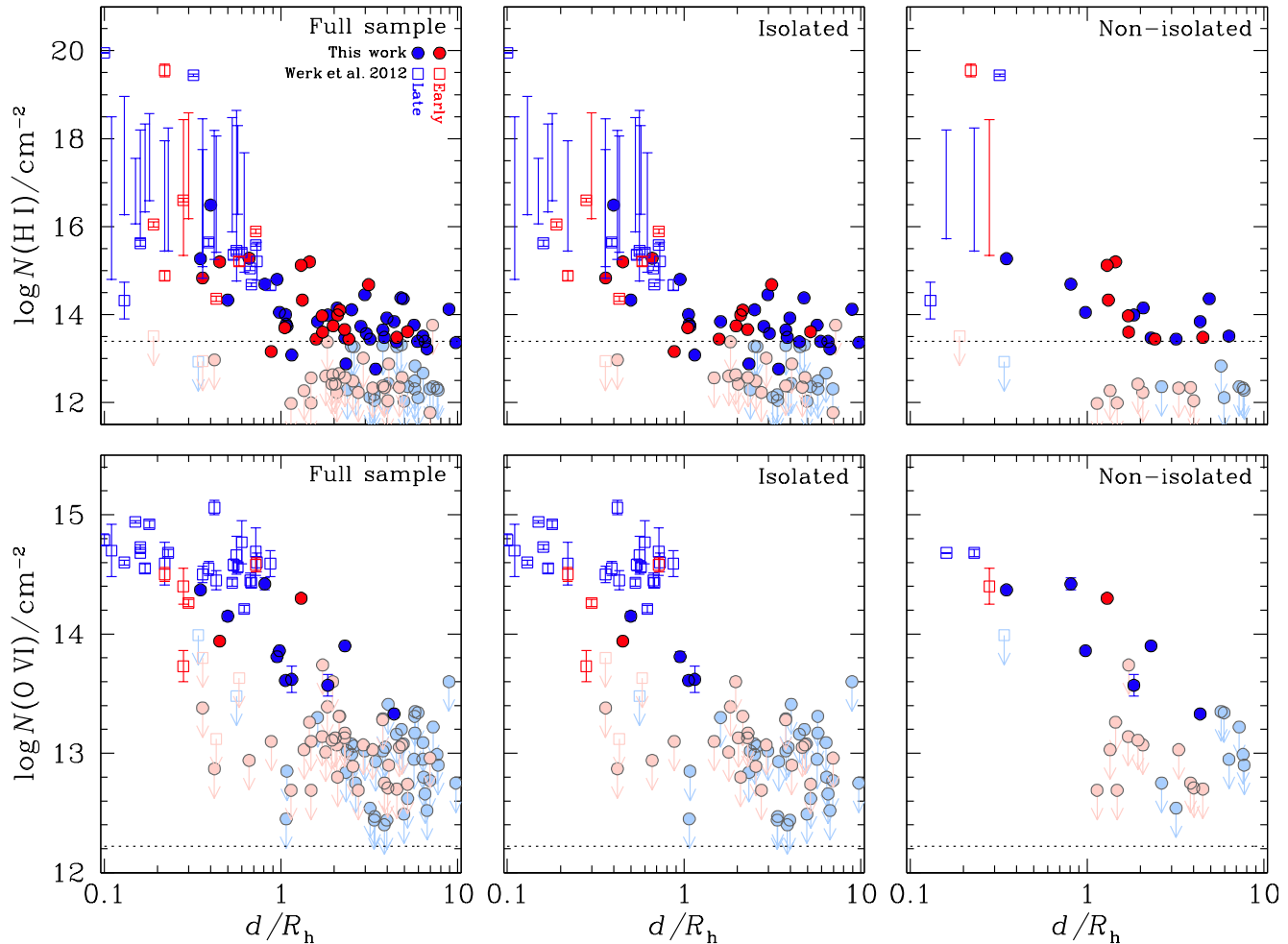


Figure 3. Column density within $\Delta v = \pm 300 \text{ km s}^{-1}$ versus projected distance measured in units of the galaxy virial radius with HI in the *top* panels and OVI on the *bottom*. The full galaxy samples are shown in the *left* column and are separated into isolated and non-isolated members in the *middle* and *right* columns respectively. Late- and early-type galaxies are shown in blue and red respectively. eCGM galaxies are displayed as filled circles and COS-Halos galaxies as open squares. Non-detections are shown as 2σ upper limits marked by downward arrows and lighter coloring. The vertical error bars represent 1σ statistical uncertainties reported by VPFIT and do not include uncertainty due to continuum placement. Galaxies with upper limits greater than $\log N/\text{cm}^{-2} = 14.0$ are not considered to have sensitive constraints on the gas column density and are not displayed. The mean absorption expected from random sightlines based on the $\frac{d^2N}{dNdz}$ measurement from Danforth et al. (2014) is shown as horizontal dotted line.

km s^{-1} for OVI. We then converted this equivalent width limit to a column density assuming that the gas is optically thin. The 75 km s^{-1} and 90 km s^{-1} integration windows correspond to the median full-width-at-half-maximum of unsaturated HI and OVI absorption components found in the eCGM survey.

For 19 galaxies, Tumlinson et al. (2013) report only lower limits on HI column density due to saturation in all available Lyman series transitions. For these galaxies, we place *upper limits* on the possible HI column density based on the lack of damping wings detected in $\text{Ly}\alpha$. To do so, we measured the $\text{Ly}\alpha$ absorption equivalent width and converted this to a HI column density upper limit assuming a single component with doppler width $b = 20 \text{ km s}^{-1}$.

4 THE EXTENT OF HI AND OVI ABSORPTION AROUND GALAXIES

With the galaxy and absorption data described in Sections 2 and 3, we characterize the HI and OVI column densities of the eCGM and COS-Halos galaxy sightlines as a function of projected distance in Figure 3. The covering fractions for strong HI and OVI absorption systems of $\log N(\text{HI})/\text{cm}^{-2} > 14.0$ and $\log N(\text{OVI})/\text{cm}^{-2} > 13.5$ are shown in Figure 4. The uncertainties in covering fractions are calculated using standard binomial statistics, and we do not include galaxies with non-detections with upper limits greater than $\log N(\text{HI})/\text{cm}^{-2} > 13.5$ or $\log N(\text{OVI})/\text{cm}^{-2} > 14.0$ in the calculations. When multiple galaxies are associated with the same absorption system, we show only the galaxy at the smallest d/R_h .

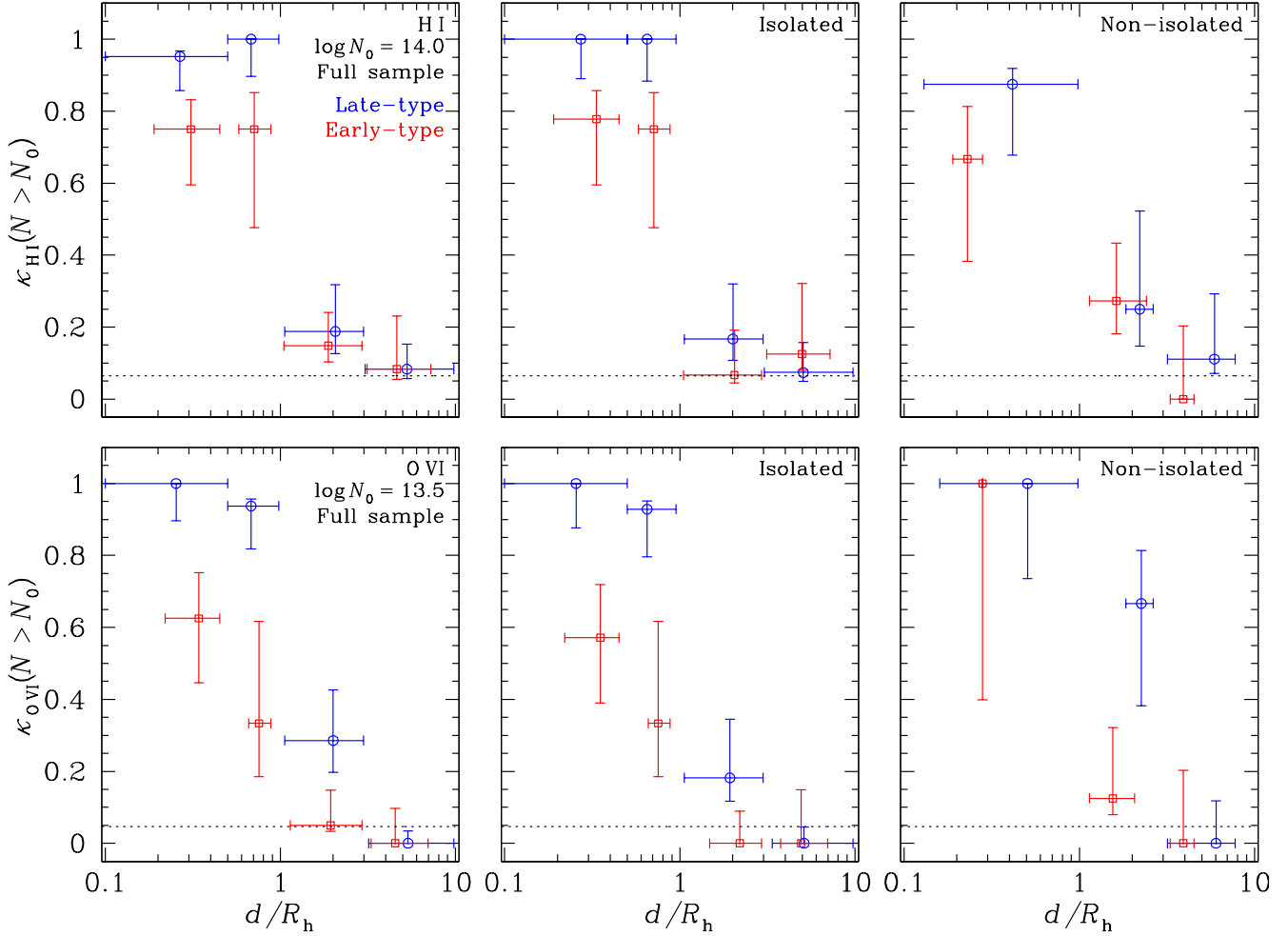


Figure 4. Covering fraction for strong HI and OVI absorption systems as a function of d/R_h . The *top* panels show the covering fraction for HI column density greater than $\log N_0(\text{HI})/\text{cm}^{-2} = 14.0$ and the *bottom* panels show the covering fraction for OVI column density greater than $\log N_0(\text{OVI})/\text{cm}^{-2} = 13.5$. The late-type galaxy samples are shown in blue and early-type in red. The full eCGM and COS-Halos samples are shown on the *left*, isolated galaxies in the *middle*, and non-isolated ones on the *right*. The horizontal error bars mark the full range of galaxies within each bin and vertical error bars represent 68% confidence intervals calculated using standard binomial statistics. We do not include non-detections with column density limits greater than N_0 in the covering fraction calculation. For both HI and OVI, we show the expected covering fraction for random sightlines based $\frac{d^2\mathcal{N}}{dNdz}$ measurements from Danforth et al. (2014).

4.1 HI

Consistent with previous surveys (e.g. Chen et al. 2001), we find a clear trend of decreasing HI column density with increasing projected distance (see the top panels of Figures 3 and 4). Lyman-limit systems (LLS) and partial Lyman-limit systems ($\log N(\text{HI})/\text{cm}^{-2} \gtrsim 16$) are common at $d < R_h$, but none are found at larger distances. Considering the eCGM and COS-Halos samples together, we identify strong HI systems with $\log N(\text{HI})/\text{cm}^{-2} > 14$ around 48 of 54 galaxies at $d < R_h$ indicating a mean covering fraction of $\langle \kappa_{\text{HI}} \rangle = 0.89^{+0.03}_{-0.06}$. At larger distances of $d/R_h = 1 - 3$ such HI absorption systems are found for only 7 of 43 galaxies ($\langle \kappa_{\text{HI}} \rangle = 0.16^{+0.07}_{-0.04}$). The HI covering fraction decreases to levels consistent with expectations from coincidental absorption systems unrelated to the galaxy survey members at $d > 3R_h$.

To determine whether galaxy environment has an influ-

ence on HI absorption far from galaxies, we show the column densities and covering fractions for isolated and non-isolated galaxies in the bottom middle and bottom right panels of Figures 3 and 4. Though the only two galaxies detected at $d > R_h$ with $\log N(\text{HI})/\text{cm}^{-2} \gtrsim 15$ have nearby neighbors, there is no clear enhancement in HI absorption in the non-isolated sample. A series of logrank tests over the range of $d/R_h = 1 - 3$ finds no evidence for differential HI absorption between the isolated and non-isolated samples. We note, however, that contamination from coincidental Ly α absorbers in the IGM is non-negligible. This contamination may obscure a difference in outer-halo HI absorption between the two samples.

Cross-correlation studies such as Chen & Mulchaey (2009) and Tejos et al. (2014) indicate that strong HI absorption systems primarily reside in the gaseous halos of star-forming galaxies. To investigate the possibility of enhanced HI absorption in galaxies with recent star-formation

activity, we show late- and early-type galaxies in blue and red respectively in Figures 3 and 4. Late-type galaxies exhibit excess HI absorption relative to early-type galaxies at projected distances of $d < R_h$. In particular, we find that 35 of 36 late-type galaxies at $d < R_h$ are associated with HI systems of $\log N(\text{HI})/\text{cm}^{-2} > 14.0$ indicating a mean covering fraction of $\langle \kappa_{\text{HI}} \rangle = 0.97^{+0.01}_{-0.06}$ compared to 13 of 18 early-type galaxies ($\langle \kappa_{\text{HI}} \rangle = 0.72^{+0.08}_{-0.12}$). However, a comparison of the distributions of HI column densities found at $d < R_h$ around late- and early-type galaxies is complicated by the poorly determined HI column densities for the LLS and partial-LLS that are common at small projected distances (see discussion in Tumlinson et al. 2013).

At larger distances of $d/R_h = 1 - 3$ the HI covering fraction for systems with $\log N(\text{HI})/\text{cm}^{-2} > 14$ are similar for late- and early-type galaxies. However, covering fractions are somewhat insensitive to the underlying HI column density distribution. To compare the HI column density distribution of late- and early-type galaxies in the outer halo, we perform a logrank test and find that the probability that the column densities around the two galaxy classes at $d/R_h = 1 - 3$ are drawn from the same underlying distribution to be $P = 2\%$. To investigate the nature of this likely differential HI absorption around late- and early-type galaxies at large projected distances, we compare the HI column densities of the two samples using the Kaplan-Meier estimator, an unbiased, non-parametric estimator of cumulative distributions in the presence of upper limits (see Feigelson & Nelson 1985) in Figure 5. We find excess HI absorption around late-type galaxies driven primarily by moderate strength absorption systems of $\log N(\text{HI})/\text{cm}^{-2} \approx 13.5$ to 14.0. Based on the Kaplan-Meier curves, we infer a median HI column density of $\langle \log N(\text{HI})/\text{cm}^{-2} \rangle \approx 13.8$ for late-type galaxies at $d/R_h = 1 - 3$. For early-type galaxies, the fraction of HI detections at these distances is too small for a robust measurement of the median, but we are able to place an upper limit on the median HI column density of $\langle \log N(\text{HI})/\text{cm}^{-2} \rangle \lesssim 13.4$.

4.2 OVI

Like HI, we find a clear anti-correlation between OVI column density and projected distance (see the bottom left panel of Figure 3). Strong OVI systems with $\log N(\text{OVI})/\text{cm}^{-2} \approx 14.5 - 15.0$ are common at $d \lesssim R_h$ but are rare at larger projected distances. OVI systems with $\log N(\text{OVI})/\text{cm}^{-2} \approx 13.5 - 14.0$ are detected out to $d/R_h = 2.3$, but at larger distances, no such strong OVI systems are found. Considering the eCGM and COS-Halos samples as a whole, we find OVI absorption with $\log N(\text{OVI})/\text{cm}^{-2} > 13.5$ for 36 of 42 galaxies at $d < R_h$ indicating a mean covering fraction of $\langle \kappa_{\text{OVI}} \rangle = 0.86^{+0.04}_{-0.07}$. Isolated galaxies exhibit OVI absorption out to $d \approx R_h$, beyond the “metal-boundary” seen in CIV and lower ions at $d \approx 0.7 R_h$. At $d/R_h = 1 - 3$ strong OVI absorption systems are found for only 5 of 34 galaxies ($\langle \kappa_{\text{OVI}} \rangle = 0.15^{+0.08}_{-0.04}$). At larger distances of $d > 3 R_h$, the OVI covering fraction decreases to levels consistent with expectations from coincidental absorption systems unrelated to the galaxy survey members (see the bottom left panel of Figure 4).

The high completeness of the galaxy survey enables a detailed investigation of possible environmental dependence

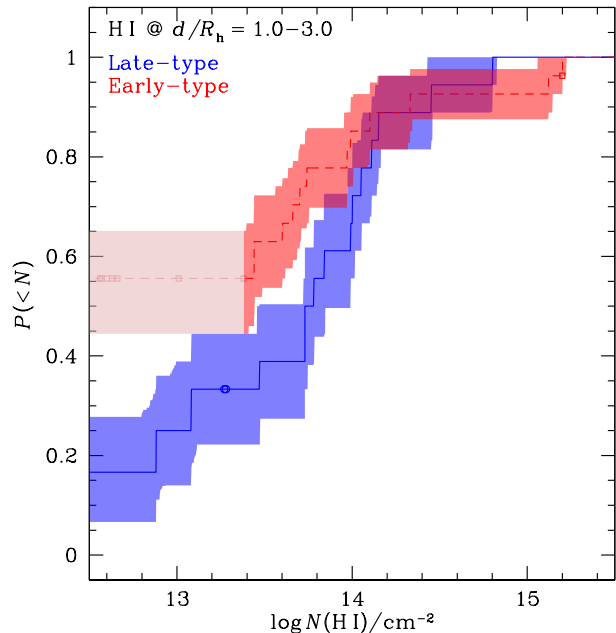


Figure 5. Cumulative fraction, P , of galaxies at $d/R_h = 1 - 3$ with total HI column densities no greater than $\log N(\text{HI})/\text{cm}^{-2}$. The late-type galaxies are shown in blue solid line and early-type as red dashed line. The cumulative distributions are estimated using the Kaplan-Meier curve, an unbiased, non-parametric estimator of the cumulative distribution in the presence of upper-limits. The Kaplan-Meier estimator changes value at detections but not at non-detections. For clarity, non-detections with upper limits are shown as open symbols. The shaded bands represent 68% confidence intervals including uncertainty due to both sample variance and column density measurement errors calculated with combined boot-strap and Monte-Carlo resampling. At column densities smaller than the highest upper limit that is less than the lowest detection, the Kaplan-Meier estimator represents an upper limit on the cumulative distribution. These column density ranges are shown in faded color.

of extended gas around galaxies, and we show OVI column density and covering fraction versus d/R_h for isolated and non-isolated galaxies separately in the bottom middle and bottom right panels of Figures 3 and 4. The decrease in incidence of strong OVI systems at $d \approx R_h$ is particularly sharp among isolated galaxies. Of the 51 isolated galaxies at $d > R_h$ in the sample we detect $\log N(\text{OVI})/\text{cm}^{-2} > 13.5$ absorption systems for only two galaxies (at $d/R_h = 1.1$ and 1.2) indicating a mean covering fraction of $\kappa_{\text{OVI}} = 0.04^{+0.05}_{-0.01}$. In contrast, three non-isolated galaxies at $d/R_h = 1.3, 1.8,$ and 2.3 are found to have absorption systems with $\log N(\text{OVI})/\text{cm}^{-2} > 13.5$ out of a sample of 24 such galaxies at $d > R_h$ ($\kappa_{\text{OVI}} = 0.13^{+0.10}_{-0.04}$). This suggests that the OVI absorption around non-isolated galaxies is more extended than around isolated galaxies.

To evaluate the possibility that non-isolated galaxies have more extended OVI absorbing gas, we compare the OVI column density distributions of the isolated and non-isolated galaxy samples at $d > 1.5 R_h$. A logrank test finds that the probability that the OVI column densities of the isolated and non-isolated galaxies at $d > 1.5 R_h$ are drawn from the same underlying distribution to be $P < 1\%$. The results of the logrank test are insensitive to the choice of

$d > 1.5 R_h$ cut-off and return a result of $P < 1\%$ over the full range of cut-off distances between 1.2 and $1.8 R_h$ and $P < 2\%$ between 1.1 and $2.2 R_h$. These findings indicate that galaxies with nearby neighbors exhibit more extended O VI absorbing gas than isolated galaxies.

Though the completeness of our galaxy survey is high, it is possible that the detections of O VI at large distances from non-isolated galaxies could be due to the presence of an additional neighbor closer to the sightline that was not observed in our survey. However, the survey incompleteness applies to the isolated and non-isolated galaxies equally. In addition, the galaxy survey completeness levels increase at small projected distances from the quasar sightline (see Figure 2 of Johnson et al. 2013). In particular, at the redshifts and distances of the non-isolated galaxies detected in O VI absorption at $d > R_h$, our galaxy survey data are $> 90\%$ complete for galaxies as faint as $0.1 L_*$.

Previous surveys (e.g. Chen & Mulchaey 2009; Tumlinson et al. 2011) found that late-type galaxies exhibit enhanced O VI absorption relative to more massive early-type galaxies at $d \lesssim 150$ kpc. We confirm that late-type galaxies show enhanced O VI absorption at $d < R_h$ relative to early-type ones. However, O VI absorption systems with $\log N(\text{O VI})/\text{cm}^{-2} > 13.5$ are found for six of eleven early-type galaxies at $d < R_h$ indicating a non-negligible covering fraction of $\langle \kappa_{\text{O VI}} \rangle \approx 0.55^{+0.13}_{-0.14}$. At larger distances of $d/R_h = 1 - 3$ we find O VI absorption with $\log N(\text{O VI})/\text{cm}^{-2} > 13.5$ for four of 14 late-type galaxies $\langle \kappa_{\text{O VI}} \rangle \approx 0.29^{+0.14}_{-0.09}$ compared to one of 19 early-type galaxies $\langle \kappa_{\text{O VI}} \rangle \approx 0.05^{+0.10}_{-0.02}$. Interestingly, the only early-type galaxy exhibiting a strong O VI system at $d > R_h$ is the brightest member of a maxBCG cluster (Koester et al. 2007) at $d = 1.3 R_h$ from the quasar sightline. A logrank test finds that the probability that the O VI column densities found at $d/R_h = 1 - 3$ from late- and early-type galaxies are drawn from the same underlying distribution to be $P = 1\%$. We note that the O VI excess in the outer halos of late-type galaxies is driven by absorption systems with $\log N(\text{O VI})/\text{cm}^{-2} \approx 13.5 - 14.0$ while the excess at smaller projected distances is driven by stronger systems with $\log N(\text{O VI})/\text{cm}^{-2} \approx 14.5$.

5 DISCUSSION

Using a highly complete survey ($\gtrsim 80\%$) of faint galaxies ($L > 0.1 L_*$) at $z < 0.4$ and $d < 500$ kpc in the fields of four COS quasar sightlines with high signal-to-noise spectra available in the *HST* archive, we have searched for the key features that determine the extended gaseous properties of galaxy halos in HI and O VI absorption. Our main findings are:

- (i) galaxies with nearby neighbors exhibit enhanced O VI absorption at $d > R_h$ relative to isolated galaxies;
- (ii) among isolated galaxies, O VI absorption extends to $d \approx R_h$, beyond the extent observed in lower ionization species such as Si III and CIV; and
- (iii) late-type galaxies exhibit enhanced HI and O VI absorption beyond characteristic halo radii at $d/R_h = 1 - 3$.

5.1 Possible environmental effect in distributing heavy elements to $d > R_h$

Among isolated galaxies without neighbors within 500 kpc and with stellar mass ratio greater than one-third, we find that O VI absorption is confined to within $d < 1.2 R_h$. None of the 18 isolated galaxies at $d/R_h = 1.2 - 3.0$ in our survey are found to have O VI absorption in the COS quasar spectrum. In contrast, three out of ten galaxies with nearby neighbors probed at $d/R_h = 1.2 - 3.0$ are found to exhibit O VI absorption with $\log N(\text{O VI})/\text{cm}^{-2} > 13.5$. On the other hand, no evidence for differential HI absorption is found between the isolated and non-isolated galaxy samples. These findings suggest that galaxy interactions play a key role in distributing heavy elements to large distances from galaxy centers, well beyond the enriched gaseous halos that surround individual galaxies.

Galaxy interactions can produce heavy elements at large projected distances through tidal stripping during satellite accretion (e.g. Wang 1993) or ram-pressure stripping (e.g. Gunn & Gott 1972). Recently, *HST* images of galaxy clusters have revealed that ram pressure stripping can remove and compress copious amounts of gas from infalling galaxies as evidenced by vigorous starbursts in debris trails (Ebeling et al. 2014). Moreover, a galaxy survey in the field of an ultra-strong Mg II absorption system near a luminous red galaxy revealed a group of evolved galaxies with no evidence of recent star-formation activity (Gauthier 2013). The lack of star-formation in the group and kinematics of the Mg II absorption are most readily explained if the Mg II absorber arises from stripped gas. Finally, in Johnson et al. (2014) we presented the discovery of a “transparent” sightline with no strong HI, Mg II or O VI absorption at $d < 20$ kpc from a pair of strongly interacting galaxies separated by a projected distance of 9 kpc. The lack of strong absorption systems detected at such small projected distance from this galaxy pair can be explained if the inner halo gas of the two galaxies has been stripped to larger distances during the galaxy interaction.

5.2 Comparison with Prochaska et al. 2011

Prochaska et al. (2011) found that galaxies at $z \lesssim 0.1$ and of $-21.1 < M_r < -18.6$ exhibit near unity covering fraction at $d < 300$ kpc and concluded that such “sub- L_* ” galaxies possess O VI bearing gaseous halos that extend to $d \approx 3 R_h$. Our highly complete galaxy survey data shed new light on these observations, indicating that O VI absorption at such large distances from galaxy halos arise in systems of multiple galaxies. Indeed, a literature search of the NASA Extragalactic database for spectroscopic neighbors reveals that all of the galaxies of $-21.1 < M_r < -18.6$ from Prochaska et al. (2011) with O VI absorption at $d \gtrsim R_h$ have neighbors within $d = 500$ kpc and satisfy our definition of a non-isolated galaxy (see Figure 6). The data from Prochaska et al. (2011) are therefore consistent with our conclusion that isolated galaxies exhibit low covering fractions at $d \gtrsim 1.2 R_h$ and support the possibility that galaxy interactions are effective at producing O VI absorbing gas at large projected distances.

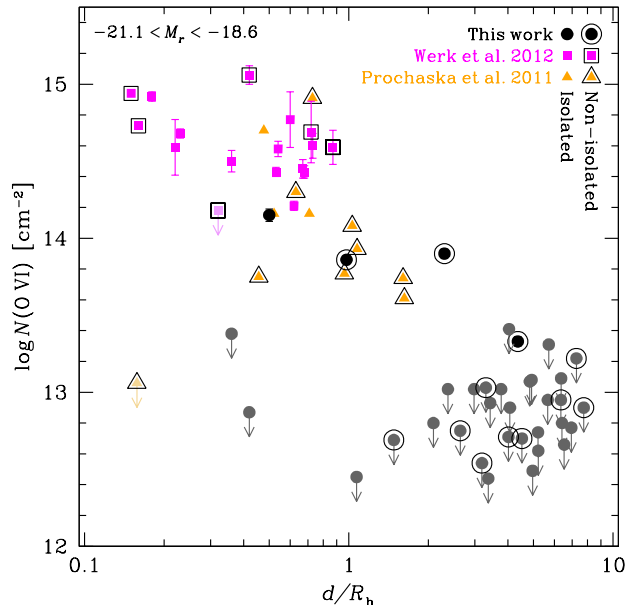


Figure 6. O VI column density versus d/R_h for sub- L_* galaxies of $-21.1 < M_r < -18.6$. Galaxies from the eCGM survey are shown as black circles, those from Werk et al. (2012) as magenta squares, and those from Prochaska et al. (2011) as orange triangles. Non-isolated galaxies are outlined by large black symbols.

5.3 O VI absorption in isolated galaxies beyond the “metal-boundary” at $d/R_h = 0.7$

Even among isolated galaxies, O VI absorption extends beyond the “metal-boundary” observed by Liang & Chen (2014) at $d = 0.7 R_h$ in lower-ionization state, enriched gas traced by absorbers such as Si II, Si III, C II, and C IV. Specifically, we find O VI absorption for seven of ten isolated galaxies at $d/R_h = 0.7$ to 1.2. The presence of O VI absorption in the outer regions of isolated galaxy halos indicates some heavy element enrichment at large radii and that highly ionized, O VI bearing clouds can form or survive in the outer halo while Si II, Si III, and C IV bearing clouds cannot. Using the mean absorption found in a stack of isolated galaxies in the eCGM and COS-Halos samples at $d/R_h = 0.7 - 1.2$, we estimate the mean metallicity of these clouds. In the stack, we measure absorption of $\log N(\text{HI})/\text{cm}^{-2} = 14.4$, $\log N(\text{O VI})/\text{cm}^{-2} = 13.9$, and place an upper limit on C III absorption of $\log N(\text{C III})/\text{cm}^{-2} < 12.6$. Assuming photoionization equilibrium models calculated with Cloudy (Ferland et al. 1998) Version 10.0, a photoionization background from Haardt & Madau (2012) at $z = 0.2$, and solar abundance patterns, these mean column densities are consistent with gas in photoionization equilibrium with ionization parameter $\log U = -1.1$ and a metallicity of one-tenth solar. The O VI and HI bearing gas may not be co-spatial allowing the ionization parameter of the HI gas to be lower. If this is the case, then the upper limit on C III absorption places stricter upper limits on the mean gas metallicity. We therefore place an upper limit of one-tenth solar on the mean metallicity of outer-halo HI gas clouds at $d \approx R_h$. This is consistent with the metallicity upper limit of one-tenth solar

found by Liang & Chen (2014) based on C IV non-detections at $d > 0.8 R_h$.

5.4 Differential HI and O VI absorption between late- versus early-type galaxies

We find excess HI and O VI absorption around late-type galaxies relative to early-type ones at $d/R_h = 1 - 3$ with 99% and 98% confidence respectively, extending previous results from Chen & Mulchaey (2009), Tumlinson et al. (2011), and Tejos et al. (2014) to larger distances. The O VI excess around late-type galaxies could be explained if the ionization mechanisms that produce O VI absorbing gas are the result of star-formation (e.g. photoionization from a young stellar population). However, this is not consistent with the observed HI excess unless the ionization mechanism is effective at producing highly ionized heavy element species but ineffective at ionizing hydrogen (e.g. Auger ionization).

Higher levels of HI and O VI absorption around late-type galaxies could be simultaneously explained if the absorption systems trace starburst driven outflows. However, simulations from Oppenheimer & Davé (2008) that incorporate strong, momentum-driven winds find that these outflows are characterized by a turnaround radius of $R_{\text{turn}} = 80 \pm 20$ kpc with only weak dependence on mass and redshift at $z < 1$. For the late-type galaxies in our survey, this corresponds to only $R_{\text{turn}}/R_h \approx 0.4$, far less than $d/R_h = 1 - 3$. Alternatively, the excess HI and O VI absorption at large distances from late-type galaxies can be explained if HI, O VI, and star-formation are observational signatures of halos in cosmic environments with multi-phase gaseous reservoirs.

The late-type members of the eCGM and COS-Halos galaxy samples are systematically less massive than the early-type members with mean stellar masses of $\log \langle M_*/M_\odot \rangle = 10.2, 10.9$ corresponding to inferred halo masses of $\log \langle M_h/M_\odot \rangle = 11.7, 12.6$ respectively. The mean doppler parameter of the HI absorption components detected at $d/R_h = 1 - 3$ from eCGM galaxies is $b = 40 \text{ km s}^{-1}$ which indicates that the HI absorbers trace cool-warm, $T \lesssim 10^5$ K gas. Our survey data are therefore consistent with a decreased incidence of cool-warm gas around more massive halos. This extends previous results from Gauthier et al. (2010) and Yoon et al. (2012) who found reduced cool-warm gas absorption in $> 10^{13} M_\odot$ mass halos relative to less massive ones. A larger sample of early-type galaxies probed in absorption is required to differentiate the effects of recent star-formation activity and mass.

ACKNOWLEDGEMENTS

We thank Michael Rauch, Gwen Rudie, Juna Kollmeier, Don York, Jean-René Gauthier, Rik Williams, Cameron Jia Liang, Daniel D. Kelson, and Andrey Kravtsov for many helpful discussions. SDJ gratefully acknowledges support from The Brinson Foundation and The Observatories of the Carnegie Institute of Washington who generously supported and hosted his studies over the last year.

This paper includes data gathered with the 6.5 meter Magellan Telescopes located at Las Campanas Observatory, Chile.

Based on observations made with the NASA/ESA Hubble Space Telescope, obtained from the Data Archive at the Space Telescope Science Institute, which is operated by the Association of Universities for Research in Astronomy, Inc., under NASA contract NAS 5-26555.

Funding for SDSS-III has been provided by the Alfred P. Sloan Foundation, the Participating Institutions, the National Science Foundation, and the U.S. Department of Energy Office of Science. The SDSS-III web site is <http://www.sdss3.org/>. SDSS-III is managed by the Astrophysical Research Consortium for the Participating Institutions of the SDSS-III Collaboration including the University of Arizona, the Brazilian Participation Group, Brookhaven National Laboratory, Carnegie Mellon University, University of Florida, the French Participation Group, the German Participation Group, Harvard University, the Instituto de Astrofísica de Canarias, the Michigan State/Notre Dame/JINA Participation Group, Johns Hopkins University, Lawrence Berkeley National Laboratory, Max Planck Institute for Astrophysics, Max Planck Institute for Extraterrestrial Physics, New Mexico State University, New York University, Ohio State University, Pennsylvania State University, University of Portsmouth, Princeton University, the Spanish Participation Group, University of Tokyo, University of Utah, Vanderbilt University, University of Virginia, University of Washington, and Yale University.

This research made use of NASA's Astrophysics Data System (ADS) and the NASA/IPAC Extragalactic Database (NED) which is operated by the Jet Propulsion Laboratory, California Institute of Technology, under contract with the National Aeronautics and Space Administration.

Funding for PRIMUS is provided by NSF (AST-0607701, AST-0908246, AST-0908442, AST-0908354) and NASA (Spitzer-1356708, 08-ADP08-0019, NNX09AC95G).

This research draws upon data provided by Brian Keeney as distributed by the NOAO Science Archive. NOAO is operated by the Association of Universities for Research in Astronomy (AURA) under cooperative agreement with the National Science Foundation.

REFERENCES

- Agertz O., Kravtsov A. V., 2014, ArXiv e-prints, 1404.2613
Ahn C. P., Alexandroff R., Allende Prieto C., Anders F., Anderson S. F., et al., 2014, ApJS, 211, 17
Behroozi P. S., Wechsler R. H., Conroy C., 2013, ApJ, 770, 57
Bernardi M., Meert A., Sheth R. K., Vikram V., Huertas-Company M., Mei S., Shankar F., 2013, MNRAS, 436, 697
Bertin E., Arnouts S., 1996, Astronomy and Astrophysics, Supplement, 117, 393
Blanton M. R., Roweis S., 2007, AJ, 133, 734
Bordoloi R., Lilly S. J., Knobel C., Bolzonella M., Kampeczyk P., et al., 2011, ApJ, 743, 10
Bordoloi R., Tumlinson J., Werk J. K., Oppenheimer B. D., Peebles M. S., Prochaska J. X., Tripp T. M., Katz N., Davé R., Fox A. J., Thom C., Ford A. B., Weinberg D. H., Burchett J. N., Kollmeier J. A., 2014, ApJ, 796, 136
Borthakur S., Heckman T., Strickland D., Wild V., Schiminovich D., 2013, ApJ, 768, 18
Bowen D. V., Blades J. C., Pettini M., 1995, ApJ, 448, 634
Bryan G. L., Norman M. L., 1998, ApJ, 495, 80
Carswell R. F., Webb J. K., Baldwin J. A., Atwood B., 1987, ApJ, 319, 709
Cen R., 2013, ApJ, 770, 139
Chabrier G., 2003, PASP, 115, 763
Chen H.-W., Helsby J. E., Gauthier J.-R., Sheckman S. A., Thompson I. B., Tinker J. L., 2010, ApJ, 714, 1521
Chen H.-W., Lanzetta K. M., Webb J. K., Barcons X., 1998, ApJ, 498, 77
—, 2001, ApJ, 559, 654
Chen H.-W., Mulchaey J. S., 2009, ApJ, 701, 1219
Coil A. L., Blanton M. R., Burles S. M., Cool R. J., Eisenstein D. J., et al., 2011, ApJ, 741, 8
Danforth C. W., Tilton E. M., Shull J. M., Keeney B. A., Stevans M., et al., 2014, ArXiv e-prints, 1402.2655
Dressler A., Bigelow B., Hare T., Sutin B., Thompson I., et al., 2011, PASP, 123, 288
Ebeling H., Stephenson L. N., Edge A. C., 2014, ApJL, 781, L40
Feigelson E. D., Nelson P. I., 1985, ApJ, 293, 192
Ferland G. J., Korista K. T., Verner D. A., Ferguson J. W., Kingdon J. B., Verner E. M., 1998, PASP, 110, 761
Ford A. B., Oppenheimer B. D., Davé R., Katz N., Kollmeier J. A., Weinberg D. H., 2013, MNRAS, 432, 89
Gauthier J.-R., 2013, MNRAS, 432, 1444
Gauthier J.-R., Chen H.-W., Tinker J. L., 2010, ApJ, 716, 1263
Green J. C., Froning C. S., Osterman S., Ebbets D., Heap S. H., et al., 2012, ApJ, 744, 60
Gunn J. E., Gott III J. R., 1972, ApJ, 176, 1
Haardt F., Madau P., 2012, ApJ, 746, 125
Hummels C. B., Bryan G. L., Smith B. D., Turk M. J., 2013, MNRAS, 430, 1548
Johnson S. D., Chen H.-W., Mulchaey J. S., 2013, MNRAS, 434, 1765
Johnson S. D., Chen H.-W., Mulchaey J. S., Tripp T. M., Prochaska J. X., Werk J. K., 2014, MNRAS, 438, 3039
Koester B. P., McKay T. A., Annis J., Wechsler R. H., Evrard A., Bleem L., Becker M., Johnston D., Sheldon E., Nichol R., Miller C., Scranton R., Bahcall N., Barentine J., Brewington H., Brinkmann J., Harvanek M., Kleinman S., Krzesinski J., Long D., Nitta A., Schneider D. P., Sneddin S., Voges W., York D., 2007, ApJ, 660, 239
Kravtsov A., Vikhlinin A., Meshcheryakov A., 2014, ArXiv e-prints
Liang C.-J., Chen H.-W., 2014, ArXiv e-prints
Loveday J., Norberg P., Baldry I. K., Driver S. P., Hopkins A. M., Peacock J. A., Bamford S. P., Liske J., Bland-Hawthorn J., Brough S., Brown M. J. L., Cameron E., Conselice C. J., Croom S. M., Frenk C. S., Gunawardhana M., Hill D. T., Jones D. H., Kelvin L. S., Kuijken K., Nichol R. C., Parkinson H. R., Phillipps S., Pimbblet K. A., Popescu C. C., Prescott M., Robotham A. S. G., Sharp R. G., Sutherland W. J., Taylor E. N., Thomas D., Tuffs R. J., van Kampen E., Wijesinghe D., 2012, MNRAS, 420, 1239
Maller A. H., Berlind A. A., Blanton M. R., Hogg D. W., 2009, ApJ, 691, 394
Maller A. H., Bullock J. S., 2004, MNRAS, 355, 694
Mathes N. L., Churchill C. W., Kacprzak G. G., Nielsen N. M., Trujillo-Gomez S., Charlton J., Muzahid S., 2014, ArXiv e-prints
McConnachie A. W., Patton D. R., Ellison S. L., Simard L., 2009, MNRAS, 395, 255
Montero-Dorta A. D., Prada F., 2009, MNRAS, 399, 1106
Moster B. P., Somerville R. S., Maulbetsch C., van den Bosch F. C., Macció A. V., Naab T., Oser L., 2010, ApJ, 710, 903
Murray N., Ménard B., Thompson T. A., 2011, ApJ, 735, 66
Oppenheimer B. D., Davé R., 2008, MNRAS, 387, 577
Prochaska J. X., Weiner B., Chen H.-W., Mulchaey J., Cooksey K., 2011, ApJ, 740, 91
Reyes R., Mandelbaum R., Gunn J. E., Nakajima R., Seljak U., Hirata C. M., 2012, MNRAS, 425, 2610
Rudie G. C., Steidel C. C., Shapley A. E., Pettini M., 2013, ApJ,

- 769, 146
- Savage B. D., Kim T.-S., Wakker B. P., Keeney B., Shull J. M., Stocke J. T., Green J. C., 2014, *ApJS*, 212, 8
- Schlegel D. J., Finkbeiner D. P., Davis M., 1998, *ApJ*, 500, 525
- Shectman S. A., Johns M., 2003, in *The International Society for Optical Engineering Proceedings*, Oschmann J. M., Stepp L. M., eds., Vol. 4837, pp. 910–918
- Shen S., Madau P., Guedes J., Mayer L., Prochaska J. X., Wadsley J., 2013, *ApJ*, 765, 89
- Stocke J. T., Keeney B. A., Danforth C. W., Shull J. M., Froning C. S., , et al., 2013, *ApJ*, 763, 148
- Stocke J. T., Keeney B. A., Danforth C. W., Syphers D., Yamamoto H., Shull J. M., Green J. C., Froning C., Savage B. D., Wakker B., Kim T.-S., Ryan-Weber E. V., Kacprzak G. G., 2014, *ApJ*, 791, 128
- Tejos N., Morris S. L., Finn C. W., Crighton N. H. M., Bechtold J., Jannuzi B. T., Schaye J., Theuns T., Altay G., Le Fèvre O., Ryan-Weber E., Davé R., 2014, *MNRAS*, 437, 2017
- Tripp T. M., Lu L., Savage B. D., 1998, *ApJ*, 508, 200
- Tumlinson J., Thom C., Werk J. K., Prochaska J. X., Tripp T. M., , et al., 2013, *ApJ*, 777, 59
- Tumlinson J., Thom C., Werk J. K., Prochaska J. X., Tripp T. M., et al., 2011, *Science*, 334, 948
- Wakker B. P., Savage B. D., 2009, *ApJS*, 182, 378
- Wang B., 1993, *ApJ*, 415, 174
- Werk J. K., Prochaska J. X., Thom C., Tumlinson J., Tripp T. M., et al., 2013, *ApJS*, 204, 17
- Werk J. K., Prochaska J. X., Thom C., Tumlinson J., Tripp T. M., O’Meara J. M., Meiring J. D., 2012, *ApJS*, 198, 3
- Wild V., Kauffmann G., White S., York D., Lehnert M., Heckman T., Hall P. B., Khare P., Lundgren B., Schneider D. P., vanden Berk D., 2008, *MNRAS*, 388, 227
- Yoon J. H., Putman M. E., Thom C., Chen H.-W., Bryan G. L., 2012, *ApJ*, 754, 84
- York D. G., Adelman J., Anderson Jr. J. E., et al., 2000, *AJ*, 120, 1579

This paper has been typeset from a $\text{T}_{\text{E}}\text{X}/\text{L}^{\text{A}}\text{T}_{\text{E}}\text{X}$ file prepared by the author.